CrossMark

ARTICLE

Development of bioceramic bone scaffolds by introducing triple liquid phases

Cijun Shuai
State Key Laboratory of High Performance Complex Manufacturing, Central South University, Changsha 410083, People's Republic of China; and State Key Laboratory for Powder Metallurgy, Central South University, Changsha 410083, People's Republic of China

Songlin Duan
State Key Laboratory of High Performance Complex Manufacturing, Central South University, Changsha 410083, People's Republic of China

Ping Wu
College of Chemistry, Xiangtan University, Xiangtan 411105, People's Republic of China

Dan Gao
School of Basic Medical Science, Central South University, Changsha 410078, People's Republic of China

Pei Feng and Chengde Gao
State Key Laboratory of High Performance Complex Manufacturing, Central South University, Changsha 410083, People's Republic of China

Shuping Peng[a)]
Key Laboratory of Carcinogenesis of the Chinese Ministry of Health, Xiangya Hospital, Central South University, Changsha 410078, People's Republic of China; Key Laboratory of Carcinogenesis and Cancer Invasion of the Chinese Ministry of Education, Cancer Research Institute, Central South University, Changsha 410078, People's Republic of China; and Hunan Key Laboratory of Nonresolving Inflammation and Cancer, Disease Genome Research Center, The Third Xiangya Hospital, Central South University, Changsha 410013, People's Republic of China

(Received 5 May 2016; accepted 13 September 2016)

In this study, a system of triple liquid phases was developed using Li_2CO_3, Na_2CO_3, and K_2CO_3 to improve the densification of the akermanite scaffolds fabricated by selective laser sintering (SLS). The system formed a ternary liquid phase (Li_2CO_3–Na_2CO_3–K_2CO_3) at 399 °C, a binary liquid phase (Na_2CO_3–K_2CO_3) at 695 °C, and a unitary liquid phase (K_2CO_3) at 891 °C during sintering process. The effects of the liquid phases on the sinterability and mechanical properties of the scaffolds were investigated. The fracture toughness and compressive strength is increased by 43 and 152% with liquid phases increasing from 0 to 4 wt%, respectively. This was explained that liquid phases enhanced densification via improving diffusion kinetics and inducing particle rearrangement. In addition, the scaffolds maintained favorable hydroxyapatite (HA) formation ability and cell proliferation ability, which was proved by simulated body fluid (SBF) test and microculture tetrazolium test (MTT), respectively.

I. INTRODUCTION

Bioceramic has attracted much attention due to the outstanding biocompatibility and bioactivity.[1–4] However, it is difficult to sinter and densify the bioceramic due to its low self-diffusion coefficient.[5,6] So the bioceramic must be sintered at a high temperature for long time to achieve a high densification.[7–9] Sintering aids is an effective choice to improve sinterability of bioceramic and obtain dense structures.[10–12] As known to all, liquid phase sintering can promote sintering and densification of ceramic.[13–15]

In general, liquid phase can improve diffusion kinetics and generate a greater capillary force,[13,16,17] which promotes the particle slip and further rearrangement thereby achieving rapid densification.[18,19] Ramesh et al.[14] and Kim et al.[20] used Bi_2O_3 and $CaO–P_2O_5–TiO_2–Na_2O$ as transient liquid phase, respectively, to improve the sinterability and densification of hydroxyapatite (HA). Vahabzadeh et al.[21] reported that lithium (Li) as a transient liquid phase was beneficial in improving the mechanical properties of β-tricalcium phosphate (β-TCP).

However, the role of a single liquid phase was limited to promote the diffusion of bioceramic during the sintering process.[22] Triple liquid phases may be more conducive to improve the mass transfer rate and mechanical properties. Potassium carbonate (K_2CO_3), sodium carbonate

Contributing Editor: Adrian B. Mann
[a)]Address all correspondence to this author.
e-mail: shuping@csu.edu.cn
DOI: 10.1557/jmr.2016.356

 © Materials Research Society 2016

https://doi.org/10.1557/jmr.2016.356 Published online by Cambridge University Press

(Na_2CO_3), and lithium carbonate (Li_2CO_3) can construct a system of triple liquid phases. It will form Li_2CO_3–Na_2CO_3–K_2CO_3 ternary liquid phase, Na_2CO_3–K_2CO_3 binary liquid phase, and K_2CO_3 unitary liquid phase at 399, 695, and 891 °C, respectively, to help densification. In addition, the Li can promote the healing of bone[23,24] and the sodium (Na) and potassium (K) as essential element of human that can improve the biological properties of the scaffolds.[25,26]

In this paper, Li_2CO_3, Na_2CO_3, and K_2CO_3 were selected as liquid phases to reinforce the akermanite ($Ca_2MgSi_2O_7$) scaffolds fabricated by selective laser sintering (SLS). The influences of liquid phases on the sinterability and mechanical properties were investigated. Moreover, the bioactivity and biocompatibility of the scaffolds were evaluated using simulated body fluid (SBF) assay, fluorescence test, and microculture tetrazolium test (MTT) assay.

II. MATERIALS AND METHODS

A. Materials and method

Akermanite powder (>98%), acquiring from Chinese New Materials Co. Ltd. (Kun Shan, China), was used as base material for this research. Li_2CO_3, Na_2CO_3, and K_2CO_3 powders (purities: 99.9%), purchasing from Alfa Aesar Co. Ltd. (Tianjin, China), were used as sintering aids. The composite powders were prepared as follows: Li_2CO_3, Na_2CO_3, and K_2CO_3 were blended in a molar ratio of 1:2:3 and followed by ball milling for 2 h in anhydrous alcohol. The slurry was dried at 70 °C for 24 h to obtain dried carbonate composite powders. Subsequently, 2, 4, and 6 wt% of the carbonate composite powders were mixed into akermanite powder followed by ball milling for 24 h in anhydrous alcohol, and then dried at 70 °C for another 24 h to achieve the composite powders.

The scaffolds were fabricated using a homemade SLS system.[27] The processing parameters were set and kept as follows: 1 mm in spot diameter, 100 mm/min in scanning speed, and 0.12 mm in layer thickness.

B. Thermal and mechanical characterization

The thermal property of the carbonate composite powders was tested by differential scanning calorimetry (DSC; STA-200 synchronous thermal analyzer, Dazhan Institute of Electronmechanical Technology, Nanjing, China) with a heating rate of 10 °C/min. X-ray diffraction (XRD; D/max 2500 X-ray diffractometer, Rigaku Corporation, Tokyo, Japan) technique was used to detect the phase composition of the scaffolds. The detection was operated at 30 mA and 30 kV with Cu K_α radiation scanning speed of 8°/min. The polished surface of the scaffolds was etched using 2% hydrofluoric acid solution for 1 min. A field emission scanning electron microscope (MIRA3 LMU, TESCAN Co., Brno, Czech Republic) was used for observing the microstructure after coating with platinum. Energy dispersive spectroscopy (EDS) system was performed to confirm the elemental composition.

The compressive strength was tested using WD-D1 desktop universal tester (Zhuoji Instruments Co., Shanghai, China) with a compressive speed of 0.5 mm/min. The fracture toughness was tested using HXD-1000 TM/LCD Vickers indentation hardness tester (Taiming Optical Instrument Co., Shanghai, China) on polished surfaces under a load of 300 gf and a holding time of 15 s. Afterward, the fracture toughness was determined according to Eq. (1)[28]:

$$K_{ic} = 0.0824\left(P/c^{3/2}\right) \quad , \tag{1}$$

where K_{ic} denotes the fracture toughness ($MPa{\cdot}m^{1/2}$), P denotes the indentation load (N), and c denotes the crack radius length (m). All test results were recorded as means ± standard deviation.

C. Biological properties characterization

Bioactivity of the akermanite scaffolds was tested in SBF.[29] The scaffolds were immersed in SBF after disinfection by ultraviolet light and then cultivated for 7, 14, and 21 days at 37 °C. The ratio of the scaffolds mass to the solution volume was 1/200 g/mL, and the solution was replaced every two days. After soaking, the scaffolds were rinsed twice with deionized water. Subsequently, the scaffolds were examined using scanning electron microscopy (SEM) with coating platinum and EDS without coating platinum.

Biocompatibility of the akermanite scaffolds was evaluated using cell culture experiment. Before cell seeding, the scaffolds were washed by deionized water and autoclaved at 125 °C for 30 min. Afterward, osteoblast-like MG63 cells (4×10^4 cells per mL) were seeded on each scaffold and put in 12-well plates. Cultivation was performed in Dulbecco's Modified Eagle's Medium which contained 10% fetal bovine serum and 1% streptomycin/penicillin, and kept a humidified atmosphere with 5% CO_2 at 37 °C.

The scaffolds were extracted from medium after culturing with MG63 cells for 1, 3, and 5 days, respectively. Afterward, the cells were rinsed with phosphate buffer saline (PBS), fixed with 4% paraformaldehyde for 10 min and permeabilized with 0.2% triton X-100 for 10 min. Next washing with PBS, the cells were cultured in PBS–0.1% bovine serum albumin (BSA) with anti-Nrf2 antibody for 2 h, and then stored overnight in the dark at 4 °C. The second day, the cells were cultured in PBS–0.2% BSA with 4 μM EthD-1 and 2 μM calcein AM for 1.5 h. Finally, the cells were directly observed by a fluorescence microscopy.

The proliferation capacity of MG63 cells on the scaffolds was quantitative measured by MTT assay. After culturing for 1, 2, 3, 4, 5, 6, and 7 days, 40 μL of

https://doi.org/10.1557/jmr.2016.356 Published online by Cambridge University Press

0.5 mg/mL MTT solution was mixed into every well to form MTT formazan. After culturing for another 4 h, dimethyl sulfoxide was mixed into every well to prevent the reaction between cells and MTT. The absorbance of every well was tested by a microplate reader.

III. RESULTS AND DISCUSSION

A. Thermal property

The thermal behavior of the carbonate composite powders was derived from DSC test (Fig. 1). Four endothermic peaks were recorded among the heating process. The first endothermic peak at 113 °C was associated with the evaporation of adsorption water.

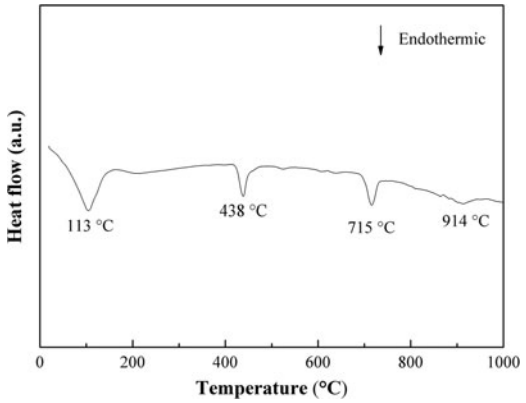


FIG. 1. DSC curve of the carbonate composite powders.

The second endothermic peak occurred at 438 °C, which is caused by the melting of the Li_2CO_3–Na_2CO_3–K_2CO_3 (molar ratio: 1:0.68:0.53) ternary powder. When the temperature reached 715 °C, another endothermic peak appeared, indicating that excessive Na_2CO_3 and K_2CO_3 further formed Na_2CO_3–K_2CO_3 (molar ratio: 1:0.63) binary eutectic. A final weak endothermic peak was noticed at 914 °C on the DSC curve, which corresponded to the melting temperature of K_2CO_3.

B. Scaffolds

The akermanite scaffold with a three dimensional structure was fabricated (Fig. 2). The dimensions of the scaffold were 16 × 16 × 6 mm^3 (length × width × height). The scaffold possessed a controlled internal and external geometric construction and an interconnected porous structure. Besides, the uniformity and connectivity of porous structure were observed by vertical view, lateral view, and front view of the scaffold (Figs. 2c and 2d). For bone repair, the porous scaffolds could help cell growth, provide pathways for biofluids, and promote nutrients transportation and metabolic waste discharge.[30–32]

C. Mechanical properties

Scaffolds would be subjected to cyclic loading when used to repair load-bearing bone defects. Thus, favorable mechanical properties such as fracture toughness and compressive strength were of crucial importance for the

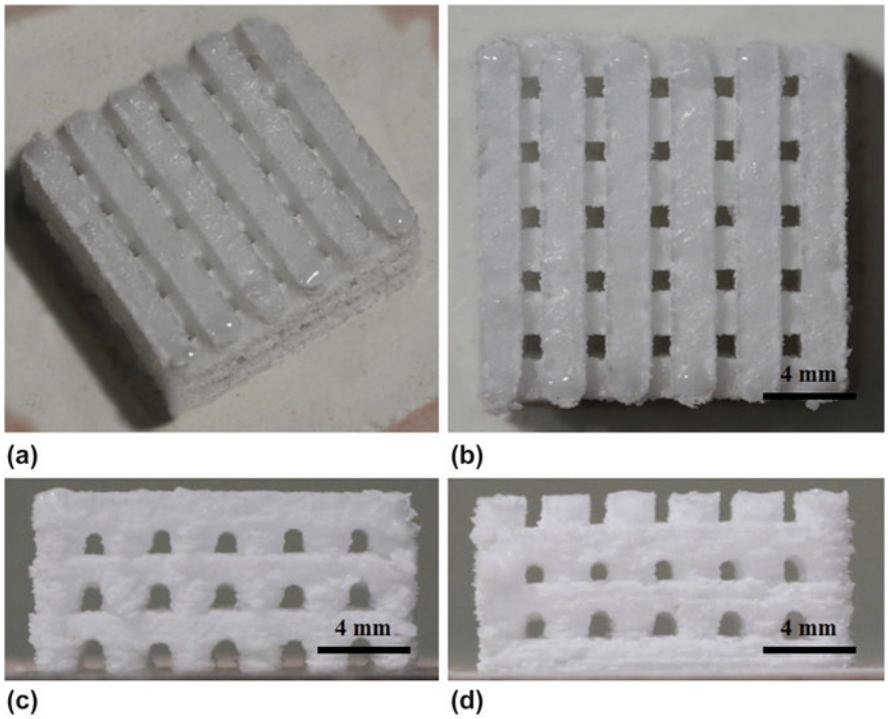


FIG. 2. The akermanite scaffold: (a) isometric view, (b) vertical view, (c) lateral view, and (d) front view.

https://doi.org/10.1557/jmr.2016.356 Published online by Cambridge University Press

scaffolds. In this study, the compressive strength was confirmed according to the stress–strain relation curves which were obtained via applying a continuous load until the scaffolds were crushed. A representative load–displacement curve after compressive test was presented in Fig. 3. The mechanical response exhibited three stages, namely elastic deformation stage, plastic flat stage, and densification stage, during the test progress. The elastic deformation stage, which associated with the scaffolds bending, showed a positive slope. In the plastic flat stage, a flat area is appeared which corresponded to scaffolds buckling. The final stage, the densification occurred and the scaffolds were broken until reaching a maximum load point.

The compressive strengths were 8.10 ± 0.25, 21.06 ± 0.48, 22.96 ± 0.15, and 20.16 ± 0.45 MPa corresponding to 0, 2, 4, and 6 wt% liquid phases, respectively, as sintered at 6 W [Fig. 4(a)]. When the scaffolds were sintered at 7 W, the compressive strength increased comparing with those of sintered at 6 W. Meanwhile, the compressive strength is increased from 10.00 ± 0.32 MPa without liquid phases to 25.21 ± 0.40 MPa with 4 wt% liquid phases (increase by 152%). When the laser power is increased to 8 W, the compressive strength is decreased slightly. The fracture toughness showed an alike trend to that of the compressive strength [Fig. 4(b)]. The test results showed that the optimal laser power was 7 W. At this sintering condition, the fracture toughness is increased from 1.62 ± 0.09 to 2.32 ± 0.12 MPa·m$^{1/2}$ (increase by 43%), as liquid phases increased from 0 to 4 wt%. And then the fracture toughness decreased to 1.93 ± 0.07 MPa·m$^{1/2}$ when liquid phases further increased to 6 wt%.

The presence of a small quantity of liquid phases (2 or 4 wt%) led to an improvement in mechanical properties, while the presence of excess liquid phases (6 wt%) decreased the mechanical properties. These were attributed to the changes of densification and microstructure. And the typical morphologies of the scaffolds with various liquid phases were presented in Fig. 5. It was obvious that akermanite was gradually sintered and the densification of the scaffolds increased with increasing liquid phases. However, in the scaffolds with 6 wt% liquid phases [Fig. 5(d)], the remarkable grain coarsening occurred [shown as black arrows in Fig. 5(d)] compared with scaffolds with 4 wt% liquid phases [shown as blue arrows in Fig. 5(c)]. As is well-known, the strength and hardness of the scaffolds follows the Hall–Petch relationship, $H_v = H_0 + kD^{-1/2}$, where H_v is the measured Vickers hardness, H_0 and k are constants, and D is the average grain size.[33] Thus, grain coarsening caused a decrease of mechanical properties. Besides, some abnormal growth of akermanite grains were observed [shown as white arrows in Fig. 5(d)], which also resulted in a decrease in the mechanical properties. This result agreed with other researcher.[34] Hence, the scaffolds with 4 wt% liquid phases were selected to perform the biological experiments.

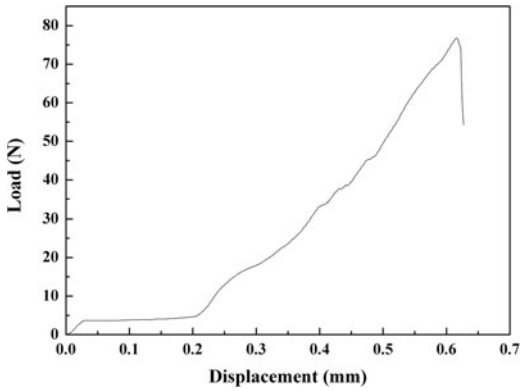


FIG. 3. The load–displacement curve of the scaffolds.

D. Phase composition

The phase composition of the scaffolds sintered at 7 W was studied using XRD (Fig. 6). The powder diffraction patterns of each composition were compared with the JCPDS file. All the characteristic peaks of akermanite

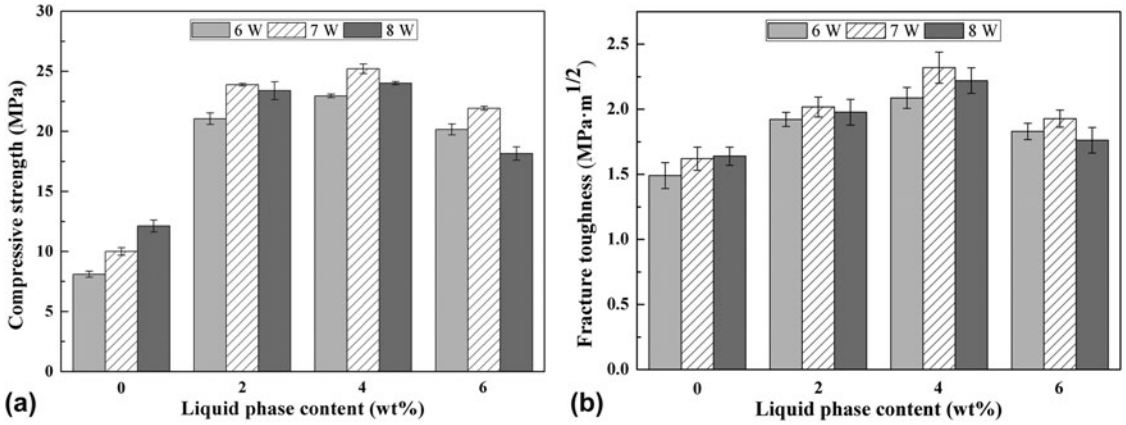


FIG. 4. The mechanical properties of the scaffolds.

https://doi.org/10.1557/jmr.2016.356 Published online by Cambridge University Press

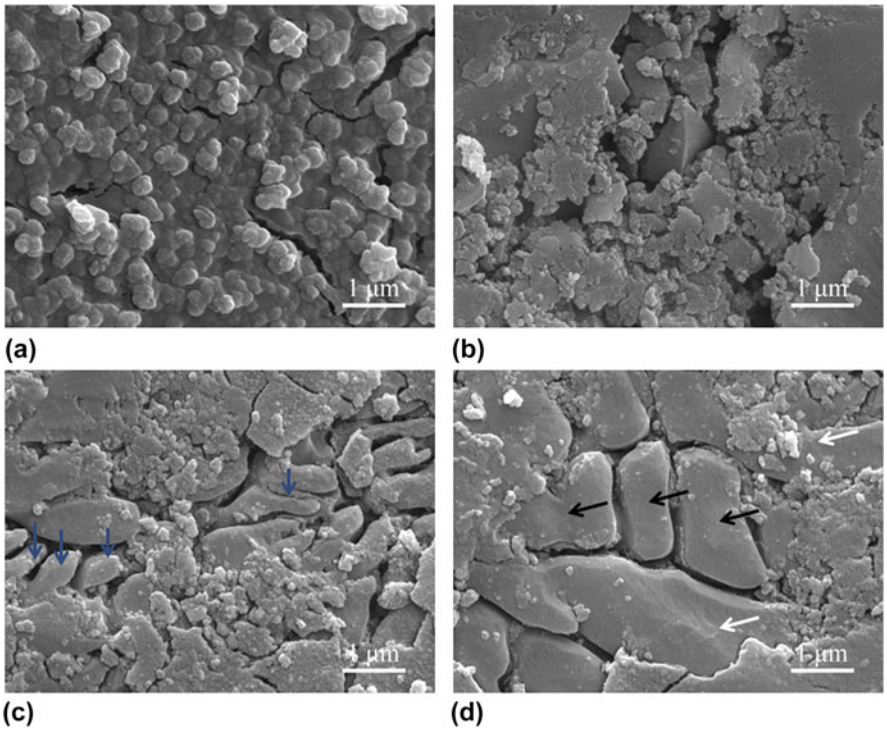


FIG. 5. Microstructure of the scaffolds with different liquid phase contents: (a) 0, (b) 2, (c) 4, and (d) 6 wt%.

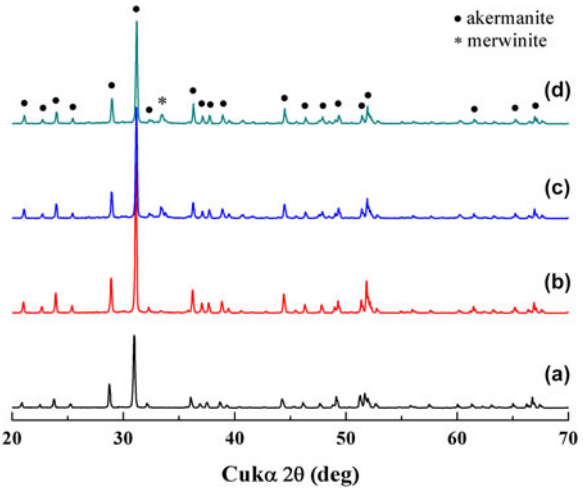


FIG. 6. XRD patterns of the scaffolds with different liquid phase contents: (a) 0, (b) 2, (c) 4, and (d) 6 wt%.

were readily confirmed in all compositions according to the standard data file (JCPDS: 35-0592). Meanwhile, an additional peak was detected as the liquid phases increased to 4 or 6% (Figs. 3c and 3d), which could be indexed to the standard data file of merwinite ($Ca_2Mg(SiO_4)_2$, JCPDS: 35-0591). The XRD results demonstrated that some reactions happened in the sintering process due to the formation of the new phase. In addition, other researcher reported that the HA layer formation and cell proliferation on merwinite ceramic were more obvious than on akermanite ceramic.[35]

E. Bioactivity

The morphologies and chemical analysis of the scaffolds, before and after immersing in SBF solution, were examined (Fig. 7). It was distinct that the scaffolds revealed a complanate feature before being exposed to SBF solution [Fig. 7(a)]. After immersion for 7 days, some precipitates appeared on the scaffolds [Fig. 7(b)]. A significant change of the morphology of the scaffolds could be observed after 14 days. The precipitates covered most of the exposed surface and a few globular precipitates are formed [shown as white arrow in Fig. 7(c)]. It further increased immersion time to 21 days, the size of globular particles increased and they dispersed gradually on the scaffolds [Fig. 7(d)].

The development of the HA layer formation on the scaffolds could also be realized in the EDS patterns. The appearance of phosphorus (P) on the scaffolds, after exposing to SBF for 7 days, indicated the HA began to form. At day 14, although the peaks of calcium (Ca) and P become strong, the presence of silicon (Si) was still obvious. It was explained that the density of HA layer was low and the akermanite matrix under the HA layer was detected. After immersion for 21 days, the peaks of magnesium (Mg) and Si became low. Meanwhile, the Ca/P ratio was 1.69 calculated according to the EDS pattern, which approached the Ca/P ratio of HA (1.67). Therefore, it was inferred that the scaffolds were almost covered completely by a thick HA layer.

https://doi.org/10.1557/jmr.2016.356 Published online by Cambridge University Press

F. Biocompatibility

Proliferation capacity of MG63 cells on the scaffolds was measured by fluorescent cell staining after culturing for 1, 3, and 5 days [Fig. 8(a)]. According to the fluorescent images, the number of cells on the scaffolds significantly increased with increasing the time periods of culture. After culture for 5 days, the cells showed a higher density and almost completely covered the scaffolds. In addition, the MTT test was performed further to quantitatively evaluate the proliferation of MG63 cells

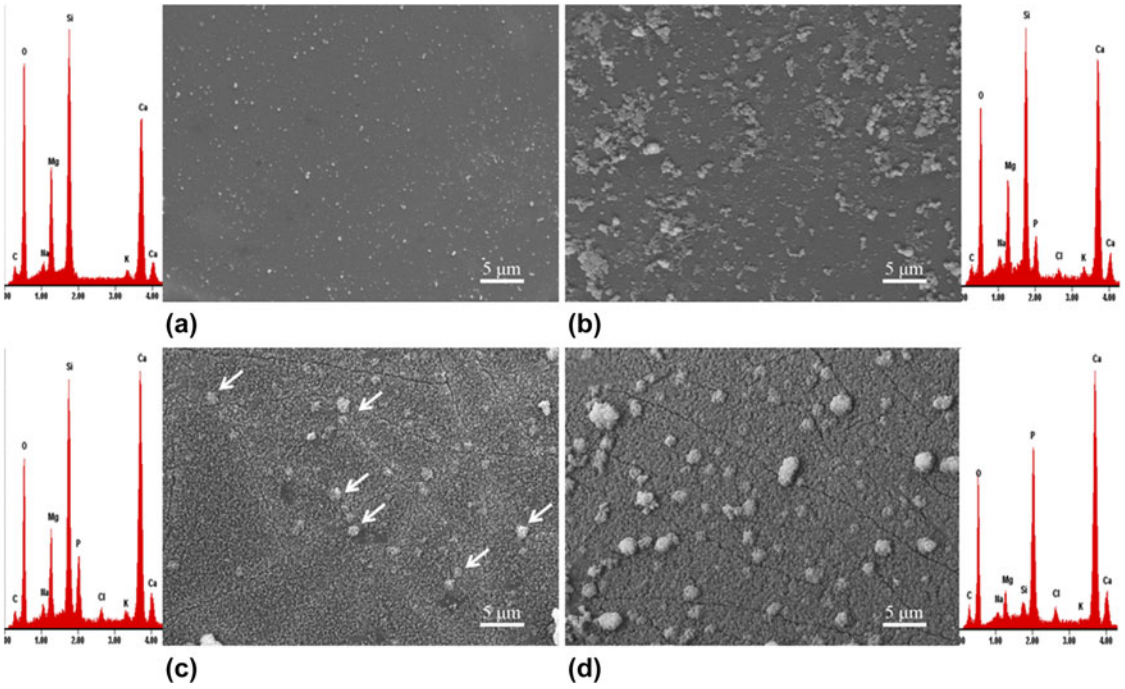


FIG. 7. Micrographs and EDS patterns of the scaffolds: (a) before immersing, and after immersing for (b) 7, (c) 14, and (d) 21 days.

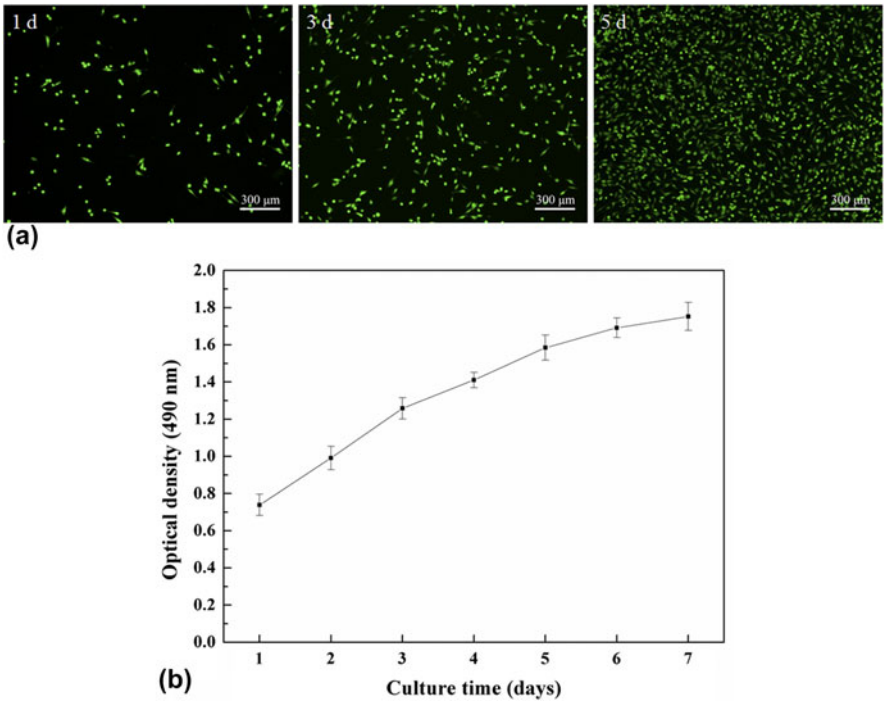


FIG. 8. Proliferation of MG63 cells on the scaffolds: (a) fluorescent cell staining after culture for 1, 3, and 5 days; (b) MTT assay of MG63 after different culture periods.

https://doi.org/10.1557/jmr.2016.356 Published online by Cambridge University Press

on the scaffolds [Fig. 8(b)]. The results indicated that the number of MG63 cells proceeded increase with extending culture time, which were in accordance with fluorescent assay.

IV. CONCLUSIONS

In this study, a porous akermanite scaffold was fabricated by introducing multiple liquid phases to promote the sintering. The compressive strength and fracture toughness is increased from 10.00 ± 0.32 MPa and 1.62 ± 0.09 MPa·$m^{1/2}$ to 25.21 ± 0.40 MPa and 2.32 ± 0.12 MPa·$m^{1/2}$ with the liquid phases increasing from 0 to 4 wt%, respectively. Furthermore, a HA layer is formed on the scaffolds after immersion in SBF. The cells could well attach and proliferate on the scaffolds. Hence, the akermanite scaffolds with multiple liquid phases may serve as an alternative for bone repair.

ACKNOWLEDGMENTS

This work was supported by the following funds: (1) The Natural Science Foundation of China (51575537, 81572577); (2) Overseas, Hong Kong & Macao Scholars Collaborated Researching Fund of National Natural Science Foundation of China (81428018); (3) Hunan Provincial Natural Science Foundation of China (14JJ1006, 2016JJ1027); (4) The Project of Innovation-driven Plan of Central South University (2015CXS008, 2016CX023); (5) The fund of the State Key Laboratory of Solidification Processing in NWPU (SKLSP201605); (6) The fund of the State Key Laboratory for Powder Metallurgy; (7) The Open-End Fund for the Valuable and Precision Instruments of Central South University.

REFERENCES

1. H. Wang, S. Zhao, X. Cui, Y. Pan, W. Huang, S. Ye, S. Luo, M.N. Rahaman, C. Zhang, and D. Wang: Evaluation of three-dimensional silver-doped borate bioactive glass scaffolds for bone repair: Biodegradability, biocompatibility, and antibacterial activity. *J. Mater. Res.* **30**, 2722 (2015).
2. D. Gopi, N. Murugan, S. Ramya, E. Shinyjoy, and L. Kavitha: Ball flower like manganese, strontium substituted hydroxyapatite/cerium oxide dual coatings on the AZ91 Mg alloy with improved bioactive and corrosion resistance properties for implant applications. *RSC Adv.* **5**, 27402 (2015).
3. C. Gao, J. Zhuang, P. Li, C. Shuai, and S. Peng: Preparation of micro/nanometer-sized porous surface structure of calcium phosphate scaffolds and the influence on biocompatibility. *J. Mater. Res.* **29**, 1144 (2014).
4. A. Aminian, K. Pardun, E. Volkmann, G.L. Destri, G. Marletta, L. Treccani, and K. Rezwan: Enzyme-assisted calcium phosphate biomineralization on an inert alumina surface. *Acta Biomater.* **13**, 335 (2015).
5. B. Gu, F. Liu, Y. Jiang, and K. Zhang: Evaluation of glass-forming ability criterion from phase-transformation kinetics. *J. Non-Cryst. Solids* **358**, 1764 (2012).
6. H. Mohammadi, M. Sepantafar, and A. Ostadrahimi: The role of bioinorganics in improving the mechanical properties of silicate ceramics as bone regenerative materials. *J. Ceram. Sci. Technol.* **6**, 1 (2015).
7. T. Tian, Y. Han, B. Ma, C. Wu, and J. Chang: Novel co-akermanite ($Ca_2CoSi_2O_7$) bioceramics with the activity to stimulate osteogenesis and angiogenesis. *J. Mater. Chem. B* **3**, 6773 (2015).
8. F.H. Perera, F.J. Martínez-Vázquez, P. Miranda, A.L. Ortiz, and A. Pajares: Clarifying the effect of sintering conditions on the microstructure and mechanical properties of β-tricalcium phosphate. *Ceram. Int.* **36**, 1929 (2010).
9. M.A. Sainz, P. Pena, S. Serena, and A. Caballero: Influence of design on bioactivity of novel $CaSiO_3$–$CaMg(SiO_3)_2$ bioceramics: In vitro simulated body fluid test and thermodynamic simulation. *Acta Biomater.* **6**, 2797 (2010).
10. C. Shuai, Z. Han, P. Feng, C. Gao, T. Xiao, and S. Peng: Akermanite scaffolds reinforced with boron nitride nanosheets in bone tissue engineering. *J. Mater. Sci.: Mater. Med.* **26**, 1 (2015).
11. P. Feng, C. Gao, C. Shuai, and S. Peng: Toughening and strengthening mechanisms of porous akermanite scaffolds reinforced with nano-titania. *RSC Adv.* **5**, 3498 (2015).
12. A.S. Sharma, N. Mishra, K. Biswas, and B. Basu: Densification kinetics, phase assemblage and hardness of spark plasma sintered Cu–10 wt% TiB_2 and Cu–10 wt% TiB_2–10 wt% Pb composites. *J. Mater. Res.* **28**, 1517 (2013).
13. R.M. German, P. Suri, and S.J. Park: Review: Liquid phase sintering. *J. Mater. Sci.* **44**, 1 (2009).
14. S. Ramesh, C.Y. Tan, W.H. Yeo, R. Tolouei, M. Amiriyan, I. Sopyan, and W.D. Teng: Effects of bismuth oxide on the sinterability of hydroxyapatite. *Ceram. Int.* **37**, 599 (2011).
15. J. Zou, G.J. Zhang, and Y.M. Kan: Pressureless densification and mechanical properties of hafnium diboride doped with B_4C: From solid state sintering to liquid phase sintering. *J. Eur. Ceram. Soc.* **30**, 2699 (2010).
16. A.L. Ortiz, O. Borrero-López, M.Z. Quadir, and F. Guiberteau: A route for the pressureless liquid-phase sintering of SiC with low additive content for improved sliding-wear resistance. *J. Eur. Ceram. Soc.* **32**, 965 (2012).
17. M.A. Malik, M.A. Hashim, and F. Nabi: Ionic liquids in supported liquid membrane technology. *Chem. Eng. J.* **171**, 242 (2011).
18. W. Wei, K. Chen, and G. Ge: Strongly coupled nanorod vertical arrays for plasmonic sensing. *Adv. Mater.* **25**, 3863 (2013).
19. M. Azadbeh, H. Danninger, and C. Gierl-Mayer: Particle rearrangement during liquid phase sintering of Cu–20Zn and Cu–10Sn–10Pb prepared from prealloyed powder. *Powder Metall.* **56**, 342 (2013).
20. T.W. Kim, S.C. Ryu, B.K. Kim, S.Y. Yoon, and H.C. Park: Porous hydroxyapatite scaffolds containing calcium phosphate glass-ceramics processed using a freeze/gel-casting technique. *Met. Mater. Int.* **20**, 135 (2014).
21. S. Vahabzadeh, V.K. Hack, and S. Bose: Lithium-doped β-tricalcium phosphate: Effects on physical, mechanical and in vitro osteoblast cell-material interactions. *J. Biomed. Mater. Res., Part B* (2015). doi: 10.1002/jbm.b.33485.
22. E.M. Ruiz-Navas, M.L. Delgado, and J.M. Torralba: 2014 based MMCs: Properties improvement by (TiCN)p and trace additions. *J. Mater. Sci.* **41**, 3735 (2006).
23. Y.T. Zeng, B. Fu, G.H. Tang, L. Zhang, and Y.F. Qian: Effects of lithium on extraction socket healing in rats assessed with micro-computed tomography. *Acta Odontol. Scand.* **71**, 1335 (2013).
24. J. Goldhahn, J-M. Féron, J. Kanis, S. Papapoulos, J-Y. Reginster, R. Rizzoli, W. Dere, B. Mitlak, Y. Tsouderos, and S. Boonen: Implications for fracture healing of current and new osteoporosis treatments: An ESCEO consensus paper. *Calcif. Tissue Int.* **90**, 343 (2012).

https://doi.org/10.1557/jmr.2016.356 Published online by Cambridge University Press

25. O. Rop, J. Mlcek, T. Jurikova, J. Neugebauerova, and J. Vabkova: Edible flowers-a new promising source of mineral elements in human nutrition. *Molecules* **17**, 6672 (2012).
26. M.Z. Kirmani, F.N. Sheikh Mohiuddin, I.I. Naqvi, and E. Zahir: Determination of some toxic and essential trace metals in some medicinal and edible plants of Karachi city. *J. Basic Appl. Sci.* **7**, 89 (2011).
27. C. Shuai, C. Gao, Y. Nie, A. Hu, H. Qu, and S. Peng: Structural design and experimental analysis of a selective laser sintering system with nano-hydroxyapatite powder. *J. Biomed. Nanotechnol.* **6**, 370 (2010).
28. S. Duan, P. Feng, C. Gao, T. Xiao, K. Yu, C. Shuai, and S. Peng: Microstructure evolution and mechanical properties improvement in liquid-phase-sintered hydroxyapatite by laser sintering. *Materials* **8**, 1162 (2015).
29. T. Kokubo, H. Kushitani, S. Sakka, T. Kitsugi, and T. Yamamuro: Solutions able to reproduce in vivo surface-structure changes in bioactive glass-ceramic A-W3. *J. Biomed. Mater. Res.* **24**, 721 (1990).
30. S. Tarafder, V.K. Balla, N.M. Davies, A. Bandyopadhyay, and S. Bose: Microwave-sintered 3D printed tricalcium phosphate scaffolds for bone tissue engineering. *J. Tissue Eng. Regener. Med.* **7**, 631 (2013).
31. F.J. O'brien: Biomaterials & scaffolds for tissue engineering. *Mater. Today* **14**, 88 (2011).
32. A. Akkouch, Z. Zhang, and M. Rouabhia: Engineering bone tissue using human dental pulp stem cells and an osteogenic collagen-hydroxyapatite-poly(l-lactide-*co*-ε-caprolactone) scaffold. *J. Biomater. Appl.* **28**, 922 (2014).
33. J.A. Wollmershauser, B.N. Feigelson, E.P. Gorzkowski, C.T. Ellis, R. Goswami, S.B. Qadri, J.G. Tischler, F.J. Kub, and R.K. Everett: An extended hardness limit in bulk nanoceramics. *Acta Mater.* **69**, 9 (2014).
34. D. Hu, Z. Li, and Y. Zhu: Effect of ZnF_2–TiO_2–SiO_2 additions on the two-step sintering behavior and mechanical properties of sol–gel derived corundum abrasive. *Ceram. Int.* **42**, 7373 (2016).
35. X. Chen, J. Ou, Y. Wei, Z. Huang, Y. Kang, and G. Yin: Effect of MgO contents on the mechanical properties and biological performances of bioceramics in the MgO–CaO–SiO_2 system. *J. Mater. Sci.: Mater. Med.* **21**, 1463 (2010).

https://doi.org/10.1557/jmr.2016.356 Published online by Cambridge University Press